Hetero-substituted $\alpha\beta$-fused BODIPY

Fabien Ceugniet, Quentin Huaulmé, Alexandra Sutter, Denis Jacquemin, Nicolas Leclerc, Gilles Ulrich

Hetero-substituted αβ-fused BODIPY

Fabien Ceugniet,[a] Quentin Huaulmé,[a] Alexandra Sutter,[a] Denis Jacquemin,[b]* Nicolas Leclerc[a]* and Gilles Ulrich[a]*

[a] Institut de Chimie et Procédés pour l'Énergie, l'Environnement et la Santé (ICPEES), UMR CNRS 7515, École Européenne de Chimie, Polymères et Matériaux (ECPM), 25 Rue Becquerel, 67087 Strasbourg Cedex 02, France. E-mail: leclercn@unistra.fr; gulrich@unistra.fr

[b] Université de Nantes, CEISAM UMR 6230, CNRS, F-44000 Nantes, France. E-mail: Denis.Jacquemin@univ-nantes.fr

Abstract:
Here we report the synthesis and properties of heterosubtituted αβfused BODIPY fluorophores. The compounds were obtained in good yields by sequential and selective Stille cross-coupling reactions from 2,3,5,6-tetrahalo-BODIPY, allowing the introduction of different subtituents at the 3,5 and 2,6 positions of the BODIPY ring. The final fused compounds were synthesized using oxidative cyclisation with ferrous chloride. The fully fused compounds show a strong bathochromically shifted emission along with a hyperchromic shift of the absorption maxima. The fluorescence quantum yields remain relatively large for compounds emitting in this wavelength range. Computational studies are planned to fully understand the photophysical behaviors of these dyes.

Introduction

Organics dyes with near-infrared (NIR) absorption and emission received a significant attention due to their numerous potential applications. For instance, dye-sensitized and bulk heterojunction solar cells, red-emitting lasers, and bio-imaging[1–3] are three areas with an intensive demand for organic dyes presenting optical properties in the NIR range. In this context, the design and the synthesis of new NIR active materials are challenges for synthetics chemists.

Fused boron dipyrromethenes, a π-extended subclass of the hallmark BODIPYs, has gained increased interest over the past decade because of their excellent optoelectronics properties in the NIR region.[4] In addition to the traditional properties of BODIPY dyes such as high molar absorption coefficient, large fluorescence quantum yield, and good photostability, fused BODIPYs display strongly redshifted absorption and emission due to the extension of their π-system. In the literature, three fused BODIPY skeleton can be identified: meso-fused[5,6], ββ-fused[7] or αβ-fused (Figure 1a-b).

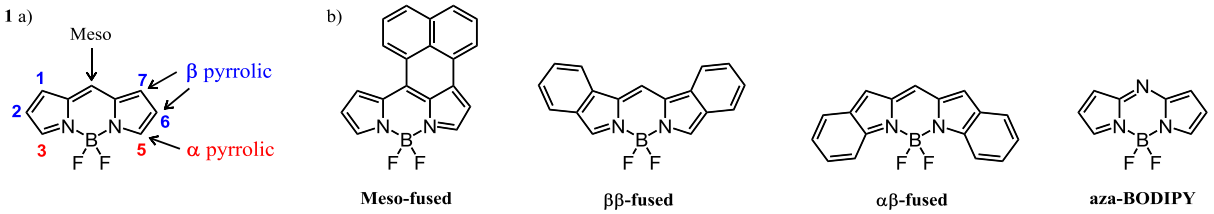

Figure 1. a) BODIPY general nomenclature b) BODIPY derivatives general skeleton

These labels indicate the position of the aromatic fused unit on the BODIPY central core. It is important to note that ββ-fused and αβ-fused aza-BODIPY have also been reported.[8,9] Among these different structures, the αβ-fused scaffolds have shown good stability and advantageously tolerate a large panel of fused substituents. These αβ-fused skeleton can be obtained by two synthetic pathways: *i*) prefunctionalisation of the pyrrole unit before the formation of the BODIPY[10] and *ii*) post-functionalizing of the BODIPY core[11]. The pre-functionalization pathway led to the formation of BODIPY with several fused units, namely a furan[12], thiophene[13] or thioenothiophene[14] at the α,β

pyrrolic positions (Figure 2), all molecules showing an intense NIR absorption. However, the synthesis of π-extended pyrrole derivatives can be cumbersome which limits the variety of available fused backbone. In contrast, when the aromatic cyclisation step occurs after the formation of the BODIPY core, i.e., when using the second (post-functionalization) strategy; the synthesis of a wide variety of fused BODIPY from a single initial BODIPY core can be attained.

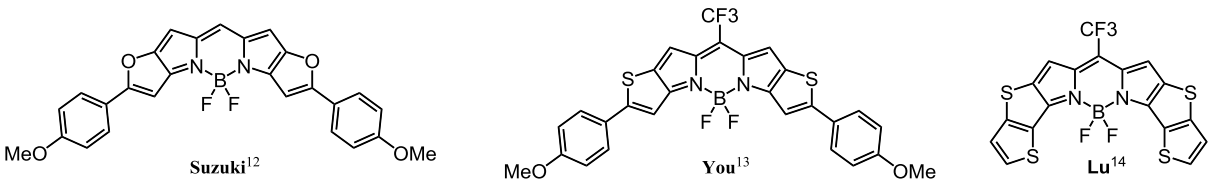

Figure 2. αβ-fused BODIPY synthesised by pre-functionalization pathway

The synthesis of several fused moieties like naphthalene,[15] indoles,[16–18] or benzofuran[19] (Figure 3) were achieved by different post-functionalization pathways. Yet, only the intramolecular oxidative ring closure strategy allowed for the formation of fused αβ-tetrasubstituted BODIPY. The initial strategy reported by Shinokubo and co-workers[20] was based on a Suzuki-Miyaura reaction between a biaryl boronic acid and a 2,6-dibromo-BODIPY followed by an intramolecular oxidative cyclisation with PIFA-BF_3·OEt_2. The main disadvantage of this method is the complexity of the biaryl boronic acid synthesis which prevents the access to a wide variety of compounds.

In 2018, our group reported a new synthetic route[21,22] that circumvents this limit by performing the key step of oxidative cyclisation between the substituents. This new method allowed us, on the one hand, to easily synthesise two isomers of homosubstituted tetrathiophene BODIPY, and, on the other hand, to differentiate the substituents introduced at the 2,6-positions from those introduced at the 3,5-positions thanks to tandem Stille coupling reactions. This paved the way to heterosubstituted fused BODIPYs. A few months later, Jiao and co-workers reported a similar method[23] to achieve the synthesis of phenenthro-fused BODIPY. Herein, we decided pushing these synthetic strategies one step further by introducing new electron-donor or electron-acceptor substituents. We report the synthesis of unprecedented homo and hetero substituted αβ-fused BODIPY dyes. The photophysical and electrochemical characterization of theses fused BODIPYs demonstrates the key role of controlling the position of the substituent in order to optimize the physico-chemical and optoelectronic properties of the final material.

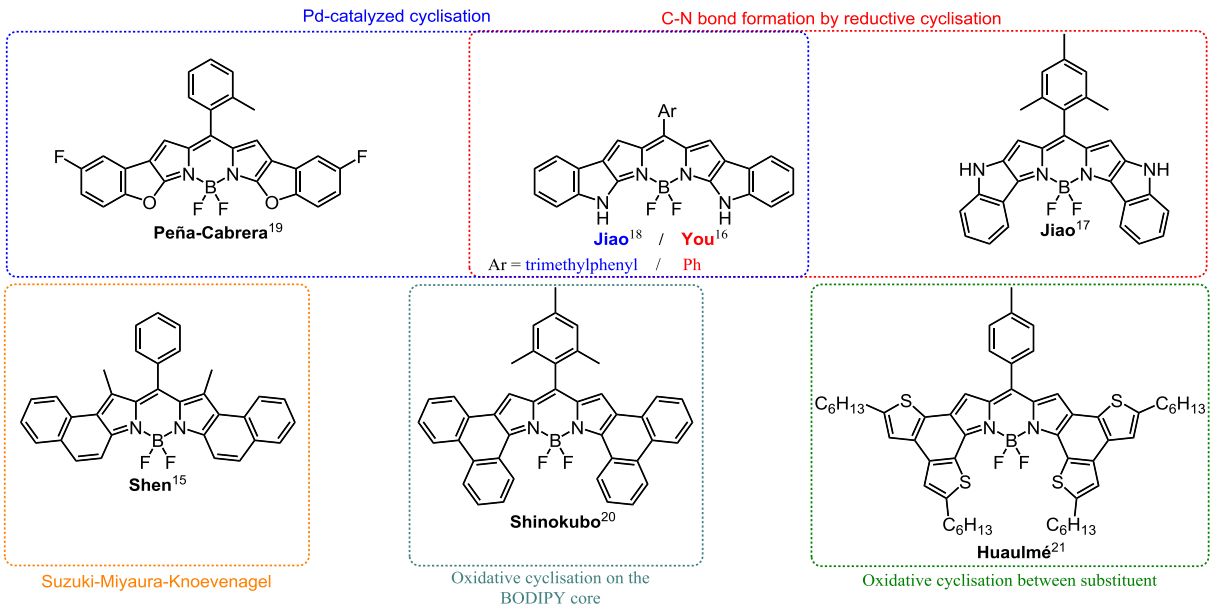

Figure 3. αβ-fused BODIPY synthesised by post-functionalization pathway and methods of cyclisation employed

Synthesis

The synthesis of 2,3,5,6-halogenated BODIPYs **1** and **4** were carried out according to the literature[21,24]. Homosubstitued BODIPYs (**2a-b**) were synthesised by cross coupling reactions from **1** with good yields for anisole and alkoxyphenyl substituents, in presence of LiCl and $Pd(PPh_3)_4$ directly in the tributylstannyl derivative as solvent (see scheme 1). Fused BODIPYs **3a** and **3b** were obtained with good yields of 62% and 55%, respectively, thanks to an intramolecular oxidative ring closure performed with an excess $FeCl_3$.

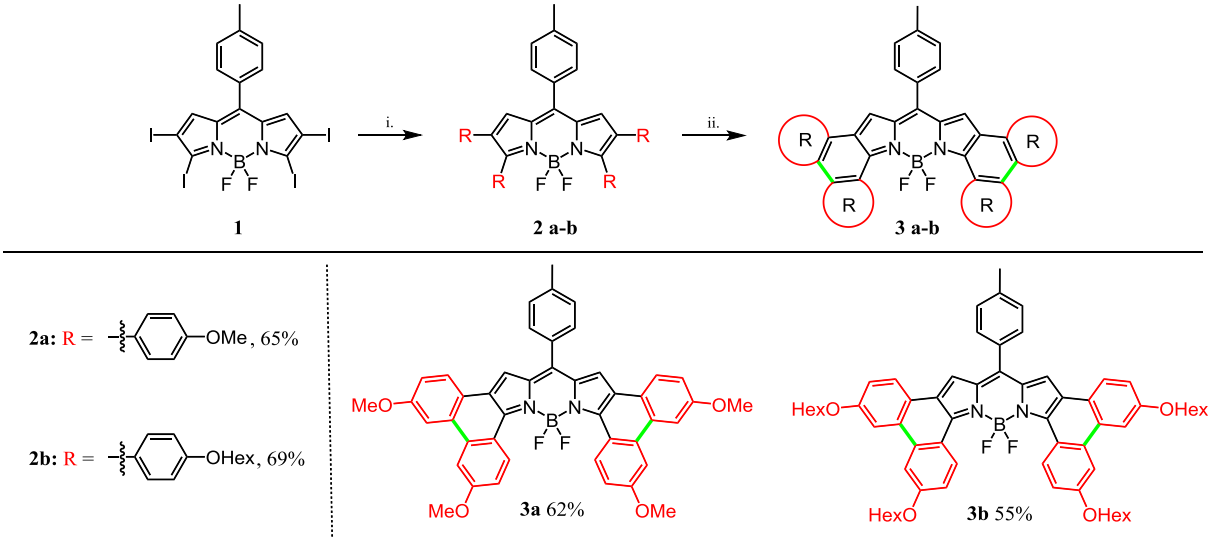

Scheme 1. Synthetic route for homosubstituted α,β-fused BODIPY: i. Stannic derivatives (15 eq), LiCl (2 eq), $Pd(PPh_3)_4$ (5% per reactive position), 130°C. ii. $FeCl_3$, DCM or DCM/$MeNO_2$

The synthetic route towards 2,6 and 3,5-heterosubstituted BODIPY is shown in Scheme 2. The was choose 2,6-dibromo-3,5-diiodo BODIPY as starting material over a tetra-homohalogenated BODIPY in order to cumulate two directional effects for Stille regioselective cross-coupling on 3,5-positions. The first guiding effect is the 3,5 positions higher reactivity toward oxidative addition in a palladium(0) catalytic mechanism compared to positions 2 and 6[25]. The second effect is the known higher reactivity of the C-I bond over the C-Br bond during Stille cross-coupling reaction.

Regioselective Stille coupling on 3,5-positions took place in very good yields (75%-89%) for anisole and thiophene derivatives with $Pd(PPh_3)_4$. In order to keep a good regioselectivity this reaction must be performed with no more than 2.5 eq of stannic derivatives. Introduction of electrodonor (anisole) or electroattractor (pyridine) moieties on **5b** by as second Stille coupling reaction can be carried out in good to very good yield. There is no problem of regioselectivity for this step so a larger excess of stannic derivatives (3.0-4.0 eq) can be used for the second coupling. Pyridines were added with different source of Pd(0) ($Pd(PPh_3)Cl_2$) than the others substituents. An excellent yield (86%) was also obtained for the introduction of thiophene substituents at the 2,6-positions of **5a** to give the BODIPY **6a.**

Then, the oxidative ring closure reaction was studied with $FeCl_3$ in DCM for each heterosubstituted BODIPY (**6a-c**). Satisfyingly, two new fused BODIPYs **7a** and **7b** were obtained in respective yields of 46% and 57%. The treatment of **6c** by $FeCl_3$ in DCM led to the slow decomplexation of the starting material. The different conditions tested for the cyclisation of **6c** are reported in Table 1. Pre-dissolution of $FeCl_3$ in $MeNO_2$ prevented the decomplexation of the starting material but did not allowed the formation of the desired compounds. Temperature increase and temporary complexation of the N pyridine atom with additive like $BF_3{\cdot}OEt_2$ or Ag_2CO_3 in order to reverse the reactivity order of the pyridine ring did not change the outcome of the reaction. The electron deficient nature of the pyridine ring and the low nucleophilicity of its position 4 could explain the non-reactivity of the compound **6c** toward the oxidative ring closure reaction with $FeCl_3$. We tried to overcome this reactivity problem by using the DDQ/CF_3SO_3H reagent couple that has been used for

the synthesis of electron-poor polyaromatic by cyclisation oxidant.[26] However, because of the poor stability of BODIPY with strong acid, this condition resulted to the rapid decomplexation of the starting material.

Table 1. Tested conditions for the cyclisation step in order to synthesise **7c**

Oxydant	Solvant	T°C	Additive	Product
$FeCl_3$	DCM	0	-	Decomplexation
$FeCl_3$	$DCM/MeNO_2$	0	-	**6c**
$FeCl_3$	$DCM/MeNO_2$	40	-	**6c**
$FeCl_3$	$DCM/MeNO_2$	40	$BF_3{\cdot}OEt_2$	**6c**
$FeCl_3$	$DCM/MeNO_2$	40	Ag_2CO_3	**6c**
DDQ	DCM	0	CF_3SO_3H	Decomplexation

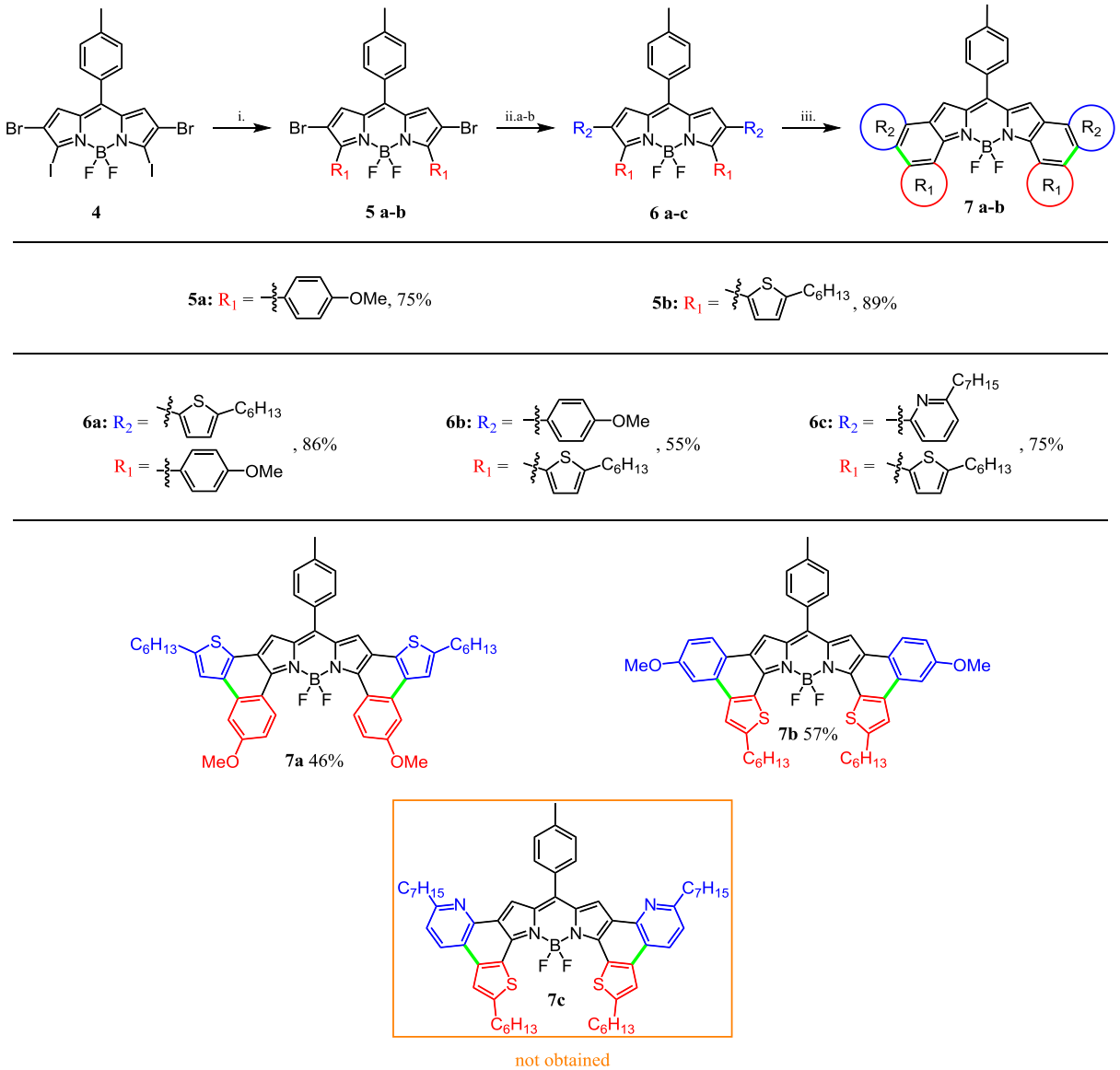

Scheme 2. Synthetic route for heterosubstituted α,β-fused BODIPY: i. Stannic derivatives (2.5 eq), $Pd(PPh_3)_4$ (5% per reactive position), PhMe, 110°C. ii. a) Stannic derivatives (4.0 eq), $Pd(PPh_3)_4$ (5% per reactive position), PhMe, 110°C. b) Stannic derivatives (3.0 eq), $Pd(PPh_3)_2Cl_2$ (5%), PhMe, 115°C. iii. $FeCl_3$, DCM or $DCM/MeNO_2$

Optical properties

All the synthesised BODIPY were characterized by absorption and emission spectroscopies. The optical data collected are summarized in the Table 2. All the BODIPYs **5** have a large and rather broad absorption band peak at ca. 600 nm. Interestingly, anisole substituent which has a strong electrodonating effect induces a smaller bathochromic shift than the thienyl substituent when they are introduced at the 3,5-positions. This effect is likely due to the stronger donating effect of the thienyls, as the geometries show no significant differences (Figure S79 in the SI). The comparison between heterosubstituted **6** and their precursor **5** shows that the introduction of additional electrodonor moieties induces slight bathochromic shifts of the absorption maxima whereas the addition of electroattractor substituent yields the opposite effect. The magnitude of the shift seems to depend on the substituents at the 3,5-positions. The absorption maxima of BODIPYs with thiophene at the 3,5 positions are only slightly red-shifted (12-17 nm in DCM) by introduction of new substituent at the 2,6 positions (from **5b** to **6b**). In contrast, 3,5 anisole substituted BODIPY see its absorption significantly impacted by the introduction of thiophene on its position 2 and 6 with a bathochromic shift of 68 nm in DCM (from **5a** to **6a**). Homosubstituted **2a-b** (Figure S64 &S65) present very similar optical properties as BODIPYs **6** (Figure S71-73) with an intense absorption band in the red region. The annulation step leads to the formation of highly structured absorption bands with strong bathochromic and hyperchromic shifts for all BODIPYs **3** and **7** (Figure 4a). These observations can be explained by the creation of a single, planar and extended π-system between the BODIPY core and its substituent. After the cyclisation step, a characteristic vibronic band of the structured BODIPY ahead of the main absorption band can be observed. This proves the rigidification of the structure after cyclisation (Figure 4a). The slightly redshift of the absorption maximum of anisole/thiophene mixed **7a-b** as compared to homosubstituted **3a-b** could hint either at better coplanarity of the π-system due to introduction of thiophene substituent, or be related the stronger donating character of the thienyl.

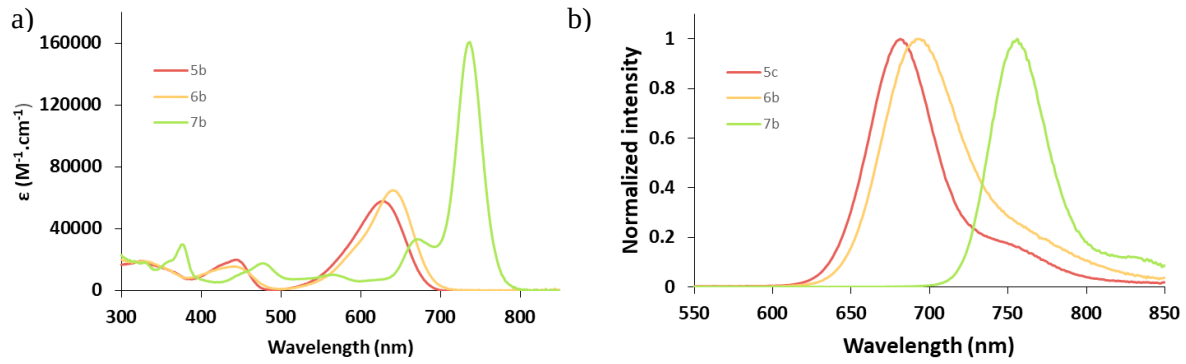

Figure 4. a) Absorption and b) emission spectra of **5b**, **6b** and **7b** in DCM (25°C)

The fluorescent quantum yields of BODIPYs **5** appeared to be heavily impacted by the nature of the substituents in 3,5 positions. In fact, thienyls substituents allow **5b** to have a quantum yield of 46%. In contrast, **5a** with anisole substituents showed low fluorescence (6%). The quantum yield difference between **5a** and **5b** is related to the 6 times higher k_{nr} in **5a**. All heterosubstituted BODIPYs **6** showed emission maxima that range from 669-720 nm. The fluorescence of BODIPYs **6** seems to be closely related to the fluorescence of their precursors **5**. Compounds **6b** and **6c** showed decent quantum yields (39 and 56% respectively) as their precursor **5b**. **5a** on its part gave the weakly fluorescent compound **6a**. Homosubstituted **2** also showed emission maxima in the red region. The weak fluorescence of **2a-b** can be explained as before by the presence of four non-fused units as substituents of the BODIPY implying higher flexibility. After the cyclisation step, the emission maximums of **3** and **7** are redshifted to the NIR region. The quantum yields of fused BODIPY **3a-b** are slightly increased and reach 20% and 25% in DCM respectively, but it is noteworthy that this increase is accompanied by redshifts, hence the fused structures allow in some sense to circumvent the *energy gap law*. This law predicts that non-radiative desexcitation are enhancing when the energy gap between the emissive excited state and the ground state is reduced due to wavefonction overlap[27]. As

their uncyclized precursor, **7a** have a low fluorescence and high k_{nr} whereas **7b** has a good fluorescence quantum yield and moderate k_{nr}. When using PhMe instead to DCM, the k_{nr} of **7** is divided by two which results into an increase of their quantum yields, this can be attributed concomitantly to the lower dielectric constant and the higher viscosity of this solvent which impact the non-radiative pathways.

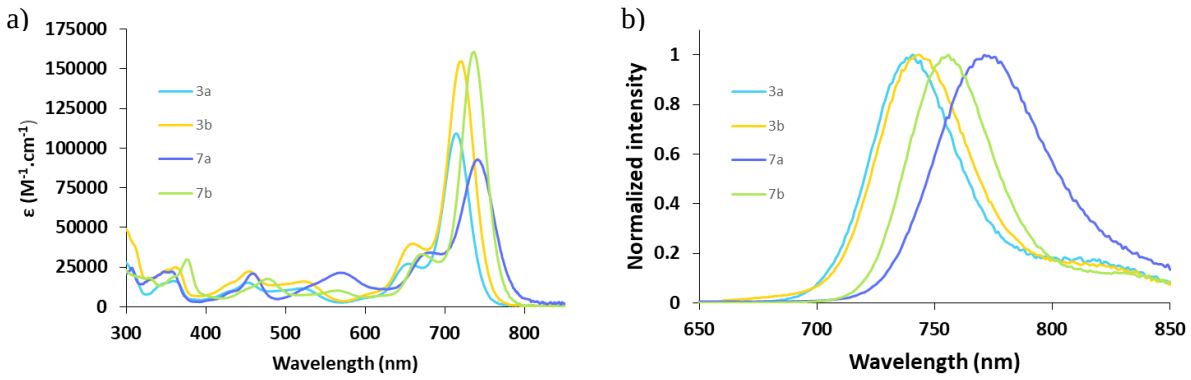

Figure 5. a) Absorption and b) emission spectra of **3b**, **7a** and **7b** in DCM (25°C)

The influence of the substituent position can be discussed by comparing two by two molecules with the same substituents, namely **6a** *versus* **6b**, and **7a** *versus* **7b**. The maximum absorption wavelength is almost not affected by the substituent position (less than 10 nm difference). For each couple, the molecule with the thienyl substituents on 3,5-positions possesses a higher molar absorption coefficient than the molecule with the same groups on 2,6-positions. Thiophene substituent on 3,5-positions also offer higher fluorescent quantum yield (at least 21% superior) and smaller Stokes' shifts. It can notice that **6b** and **7b** present a twice larger k_r and keep a relatively low k_{nr} , despite the presence of two substituents at 2,6-positions with a methoxy group, compared to their **a** counterparts. This suggests that the influence of methoxy group on the k_{nr} is also dependent of the substituents position on the BODIPY core. From these comparisons, the introduction of a thiophene moieties on 3,5-position seem to be preferable than an anisole substituent in order to increase the NIR absorption and brightness of the molecule.

Table 2. Spectroscopy data recorded at 25°C [a] HCl vapor were bubbled into the solution.

Product	λ_{abs} (nm)	ε ($M^{-1}.cm^{-1}$)	λ_{em} (nm)	φ_F	τ (ns)	k_r (10^8 Hz)	k_{nr} (10^8 Hz)	Δ_{SS} (cm^{-1})	E^{00} (eV)	Solvent
2a	612	33800	667	0.15	3.0	0.51	2.9	1348	1.94	DCM
2b	615	71500	673	0.17	2.6	0.66	3.2	1401	1.93	DCM
5a	580	61000	623	0.09	1.7	0.53	5.4	1190	2.01	DCM
5b	629	59500	681	0.46	6.1	0.75	0.88	1214	1.88	DCM
6a	648	49000	720	0.04	1.0	0.39	9.4	1534	1.81	DCM
6b	641	64700	693	0.39	5.9	0.66	1.0	1170	1.86	DCM
6c	611	68000	669	0.56	5.7	0.98	0.77	1419	1.93	DCM
	585	70300	649	0.44	4.7	0.94	1.2	1686	-	DCM + HCl (vap)
3a	713	128000	740	0.20	4.8	0.42	1.7	512	1.71	DCM
	Insoluble									Toluene
3b	720	154700	742	0.25	4.9	0.51	1.5	412	1.70	DCM
	724	205000	739	0.37	6.1	0.61	1.0	280	1.70	Toluene

7a	742	92600	770	0.05	1.5	0.33	6.3	490	1.64	DCM
	744	101100	765	0.10	2.3	0.44	4.0	369	1.64	Toluene
7b	736	160500	755	0.26	2.8	0.92	2.6	342	1.66	DCM
	740	197700	753	0.37	7.1	0.52	0.89	233	1.66	Toluene

Among the synthesized BODIPYs, **6c** has the additional property of being pH sensitive due to the facile protonation of its pyridine moieties. The absorption and emission properties of the neutral and protonated forms of **6c** are in the red region, their average to good fluorescent quantum yield (56% for the neutral form, 44% for the protonated) and the 20 nm difference between the emission maxima of the both forms can make the 2,6-pyridine-3,5-thiophene BODIPY skeleton an interesting candidate for the development of ratiometric sensors of which it is a prototype example of a pH probe.

Theoretical modelling

To shine a complementary light on these compounds, first principles calculations on the various dyes using an approach based on CC2 transition energies and TD-DFT structures have been performed.[28] The method used is detailed in the SI. Main results are reported in Table 3. We first note that the computed absorption and emission wavelengths are obtained in the vertical approximation and hence cannot be directly compared to experiment. However, their evolution across the series qualitatively follows the experimental trends (compare the evolution in Tables 2 and 3). To have a more direct comparison between the measurements and the theoretical calculations, one can compare the computed 0-0 energies to the experimental crossing point between the absorption and emission curves. Such a comparison yields a mean absolute deviation of 0.098 eV and a very high determination coefficient (R^2=0.99). Likewise, the computed ZPVE-corrected Stokes shifts are of the same order of magnitude as the measured ones (mean absolute deviation 94 cm^{-1}), follows exactly the same trends as experiment (R^2=0.95) with noticeable decreases when going to ring-fused systems. These values confirm the quality of the theoretical simulation. Interestingly, the data of Table 3 reveal that **7c**, that could not be accessed synthetically would very likely present significantly blueshifted absorption and emission as compared to both **7a** and **7b**.

Table 3. Theoretical data determined using a mixed CC2/PCM-TD-DFT protocol in dichloromethane: vertical absorption and emission wavelengths, 0-0 energies, and Stokes shift based on the vertical values and corrected for ZPVE effects. On the right hand side, key dihedral angles computed are provided in both electronic states.

Product	λ_{abs}^{vert} **(nm)**	λ_{fluo}^{vert} **(nm)**	E^{00} **(eV)**	Δ_{SS} **(cm^{-1})**	φ_{3-5}^{S0} **(deg)**	φ_{3-5}^{S1} **(deg)**	φ_{2-6}^{S0} **(deg)**	φ_{2-6}^{S1} **(deg)**
2a	591	653	1.851	1292	48	38	42	38
3a	677	720	1.633	399	5	5	0	0
5a	569	627	1.953	1291	46	37	-	-
5b	605	668	1.775	1154	35	22	-	-
6a	615	691	1.727	1438	47	42	35	29
6b	606	670	1.742	1142	44	27	44	47
6c	567	644	1.824	1684	54	30	28	38
7a	699	748	1.552	406	3	3	1	1
7b	693	730	1.587	295	0	0	0	0
7c	644	679	1.720	1292	0	0	0	0

In Table 3, the main dihedral angles between the substituents at 3,5 and 2,6 positions and the fluoroborate core in both electronic states are reported. As can be seen in the non-fused systems, namely **2a**, **5a**-**b** and **6a-c**, there is a clear trend of more coplanar systems in the lowest excited-state, especially for the rings at 3,5, which explains the significant Stokes shifts in these systems. As expected the ring-fused systems are almost perfectly planar, and the thienyl groups are less twisted than their phenyl counterparts (e.g., compare **5a** and **5b**). It can be note that **7b** is the most perfectly

planar structure, with negligible out-of-plane deformations in both the ground and the excited-state. In contrast **7a**, is slightly departing from planarity, in both states and also undergoes a small yet non-trifling excited-state planarization. This is well in line with the very small Stokes shift for **7b** (both experimentally and theoretically), as well as for the significantly smaller k_{nr} in **7b** than in **7a** (see Table 2).

In Figure 6, we provide density difference plots for selected compounds. The general topology of the excited states are similar to the one of BODIPY and cyanines,[29] but nevertheless reveals interesting differences between the various dyes. First, in the ring-fused **3a**, one notices a rather limited contribution from the anisole groups that act as secondary donor groups, with an excited-state topology highly similar to the one found in **2a**, indicating that it is indeed the planarization that induces the redshifts of the absorption and emission, rather than a stronger role of the anisoles. When comparing now **6a** and **6b**, one clearly sees that the thienyl rings participate more significantly in the excited state than the anisole groups, irrespective of their position, confirming their leading donor effect. This effect takes place even in **6b** in which there is a significant twist of the thienyls in the ground state (see Table 3), and cannot be attributed to a geometric effect only. The trends noted in **6a** and **6b** are found again in **7a** and **7b**, although the excited-state are more spread in the ring-fused dyes.

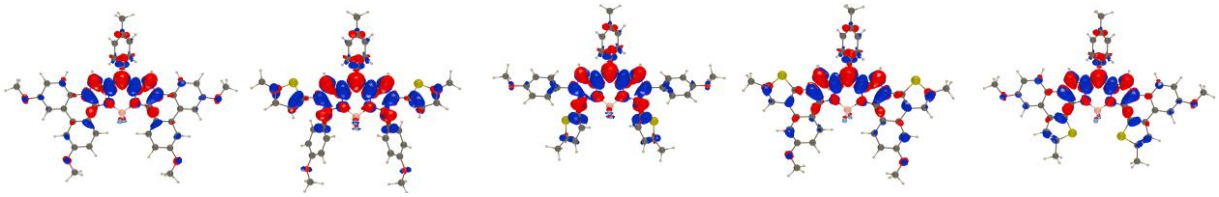

3a **6a** **6b** **7a** **7b**

Figure 6. Density difference plots for selected compounds (see the SI for all structures, figure S80). The blue and red lobes correspond to regions of increase and decrease of electronic density respectively. Contour threshold 8×10^{-4} au.

Electrochemistry

Cyclic voltamperometry was used to investigate the oxidation and reduction potential of the new compounds in CH_2Cl_2 solutions. Potentials are given *versus* a saturated calomel electrode (SCE). Then, the energies of the highest occupied molecular orbital (HOMO) and lowest unoccupied molecular orbital (LUMO) levels were extracted using the following formulas: LUMO (eV) = -[E_{onset}^{Red} (vs SCE) + 4.4] and HOMO=-[E_{onset}^{Ox} (vs SCE) + 4.4] (see the SI for experimental details).

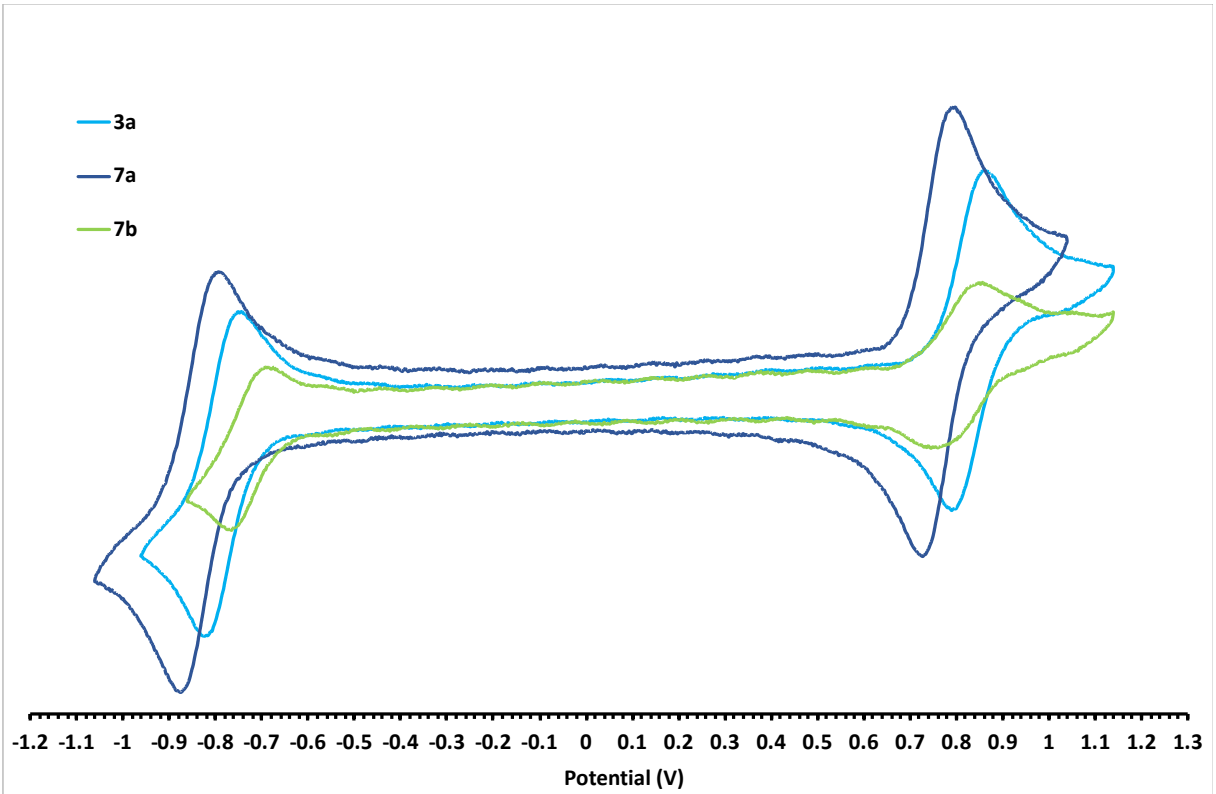

Figure 7. Cyclic voltammograms of 3a (light blue), 7a (dark blue) and 7b (green) in DCM solution + $TBAPF_6$ 0.1 M; (Sweep-rate: 150 $mV.s^{-1}$, platinum wire working electrode).

All materials exhibit reversible oxidation and reduction waves in very similar ranges of potential. **3a** shows oxidation and reduction potentials at -5.14 eV and -3.69 eV, respectively. When going from **3a** to **7a**, by replacing the anisole groups in 2,6-positions by alkylated thiophene ones, both processes were observed at slightly lower potentials. Interestingly, reverse the position of the anisole and thiophene units in compound **7b** leads to positive shift of both oxidation and reduction processes. Consequently, **7b** exhibits the highest electron affinity and an ionization potential almost identical to the one of **3a** (see Table 4).

Table 4. Cyclic voltammetry data

Product	E_{onset}^{Ox} (V vs SCE)	E_{onset}^{Red} (V vs SCE)	HOMO (eV)	LUMO (eV)	ΔEg^{CV} (eV)
3a	0.74	-0.71	-5.14	-3.69	1.45
7a	0.68	-0.76	-5.08	-3.64	1.44
7b	0.72	-0.66	-5.12	-3.74	1.38

Done in deoxygenated CH_2Cl_2 containing $TBAPF_6$ (0.1 M), and a solute concentration of $1\text{-}5\times10^{-3}$ M at 25 °C. The LUMO and HOMO levels were estimated from the following equations, using the oxidation and reduction onset potentials: LUMO (eV) = −[E_{onset}^{red} (vs SCE) + 4.4] and HOMO (eV) = −[E_{onset}^{ox} (vs SCE) + 4.4], based on an SCE energy level of 4.4 eV relative to the vacuum.

Conclusion

In summary, the synthesis strategy we have recently developed to access αβ-fused BODIPY molecules was further explored. This rather versatile synthesis strategy enables to consider different (hetero)aromatic substituents but also to reach unsymmetrical αβ-fused BODIPY molecules, through the selectivity of the Stille coupling on the 3,5 and 2,6-positions of the tetraheterohalogenated

BODIPY core. All molecules exhibit highly appealing optical absorption and emission properties. However, we have shown that the nature of the aromatic substituents used obviously impacts these properties, allowing the finetuning of the absorption and emission ranges over a wide scale. In addition, in the case of unsymmetrical BODIPYs, the position of each of the substituents allows these properties to be further controlled.

Finally, the extremely planar nature of these fused molecules makes it possible to achieve the NIR absorption and emission, which is highly desired for bio-medical imaging applications, but also to achieve high charge transport properties, which is very promising for applications in organic optoelectronics.

Accordingly, we strongly, believe that these properties, together with the rather easy, versatile and high-yielding synthesis route, open up a bright future for these αβ-fused BODIPY molecules.

Experimental section

The synthesis of the organotin derivatives, **2b, 3b, 5b**, **6b**, **6c** and **7b** are described in the supporting information.

General procedure 1 : Stille cross-coupling reactions
In a dried Schlenk tube were added the appropriate halogenated (1.0 eq) and stannic derivatives (2.0 eq per reactive position). Anhydrous toluene was added and the mixture was degassed for 30 min with Ar. $Pd(PPh_3)_4$ (5% per reactive position) was added and the mixture heated at 110°C for the indicated time.

General procedure 2: oxidative ring closure reactions
To a stirred solution of tetrasubstituted BODIPY derivative in dry DCM (BODIPY concentration~ 1 $mmol.L^{-1}$) was added at 0°C anhydrous $FeCl_3$. The mixture was stirred for the indicated temperature at the indicated time. The reaction was quenched by addition of water. The aqueous layer was extracted with DCM. The combined organic layer was washed with water, brine, and was then dried over $MgSO_4$. Column chromatography on silica followed by a recrystallization.

Synthesis of 2a
According to ***General Procedure 1***, without solvent and with an excess of raw stannic derivative **A1** (15 eq) in presence of lithium chloride (2.0 eq). The reaction mixture was heated at 130°C for 3 h. Starting from **1** (400 mg, 0.509 mmol, 1.0 eq), column chromatography (PE/DCM 2:3 to 1:4) followed by trituration in ACN afforded the pure product as a blue solid (233 mg, 0.331mmol, 65%). **^{1}H NMR** (400 MHz, $CDCl_3$): δ = 7.56 (d, J = 7.8 Hz, 2H), 7.43 (d, J = 8.6 Hz, 4H), 7.35 (d, J = 7.8 Hz, 2H), 6.95 (d, J = 8.6 Hz, 4H), 6.84 (d, J = 8.5 Hz, 4H), 6.92 (s, 2H), 6.71 (d, J = 8.5 Hz, 4H), 3.81 (s, 6H), 3.75 (s, 6H). **^{13}C NMR** (100 MHz, $CDCl_3$): δ = 160.2, 158.7, 155.8, 155.7, 143.7, 142.5, 140.6, 134.7, 134.1, 132.2, 132.0, 130.9, 129.7, 129.2, 127.9, 127.8, 126.9, 126.1, 124.5, 113.7, 113.5, 55.4, 55.3, 21.6. **^{11}B NMR** (128 MHz, $CDCl_3$): δ = 1.06 (t, J_{B-F} = 31.4Hz). **^{19}F NMR** (376 MHz, $CDCl_3$): δ = -132.9 (q, J_{F-B}=31.4Hz). **HRMS** (ESI-TOF): calcd for $C_{44}H_{37}BF_2N_2O_4$ $[M]^+$, 706.2816; found 706.2813.

Synthesis of 3a
According to ***General Procedure 2***, starting from **2a** (110 mg, 0.156 mmol, 1.0 eq). The reaction mixture was stirred 4 h at R.T. Column chromatography (DCM) followed by recrystallization from DCM/EtOH afforded the pure **3a** (68 mg, 0.0967 mmol, 62%) as a black solid. **^{1}H NMR** (400 MHz, $CDCl_3$): δ = 9.6 (d, J = 9.5 Hz, 2H), 7.89-7.91 (m, 4H), 7.79 (s, 2H), 7.62 (d, J = 7.6 Hz, 2H), 7.39-

7.43 (m, 4H), 7.35 (s, 2H), 7.11 (d, J = 9.5 Hz, 2H), 4.07 (s, 6H), 3.97 (s, 6H), 2.56 (s, 3H). **^{13}C NMR** (126 MHz, $CDCl_3$) δ = 160.74, 158.72, 149.13, 142.67, 140.40, 138.55, 135.93, 132.64, 131.48, 131.39, 129.69, 129.48, 129.17, 125.65, 121.75, 121.20, 118.61, 116.25, 115.00, 108.37, 106.92, 55.73, 55.68, 21.69. **^{11}B NMR** (128 MHz, $CDCl_3$): δ = 2.86 (t, J_{B-F}=35.2Hz). **^{19}F NMR** (376 MHz, $CDCl_3$): δ = -139.2 (q, J_{F-B} =35.4Hz). **HRMS** (ESI-TOF): calcd for $C_{44}H_{33}BF_2N_2O_4$ $[M]^+$, 702.2501; found 702.2512.

Synthesis of 5a

According to ***General Procedure 1*** in presence of 2.5 eq of raw stannic derivative **A1**. The reaction mixture was heated for 16 h. Starting from **4** (317 mg, 0.460 mmol, 1.0 eq), column chromatography (PE/DCM 1:1) afforded the pure product as a blue solid (225 mg, 0.345 mmol, 75%). **^{1}H NMR** (400 MHz, $CDCl_3$) δ = 7.61 (d, J = 8.4 Hz, 4H), 7.47 (d, J = 7.9 Hz, 2H), 7.37 (d, J = 7.9 Hz, 2H), 7.00 (s, 2H), 6.95 (d, J = 8.6 Hz, 4H), 3.84 (s, 6H), 2.50 (s, 3H). **^{13}C NMR** (100 MHz, $CDCl_3$): δ =160.89, 155.90, 141.44, 134.28, 132.08, 131.72, 130.87, 130.67, 129.48, 122.48, 113.54, 55.35, 21.64. **^{11}B NMR** (128 MHz, $CDCl_3$): δ = 0.67 (t, J_{B-F} = 29.9 Hz). **^{19}F NMR** (376 MHz, $CDCl_3$): δ = -133.4 (q, J_{B-F} = 29.9 Hz). **HRMS** (ESI-TOF): calcd for $C_{30}H_{23}BBr_2F_2N_2O_2$ $[M]^+$, 652.0169; found 652.0133.

Synthesis of 6a

According to ***General Procedure 1*** in presence of 4.0 eq raw stannic derivative **T**. The reaction mixture was heated for 16 h. Starting from **5a** (112 mg, 0.172 mmol, 1.0 eq), column chromatography (PE/DCM 3:2) and recrystallization from THF/Pentane afforded the pure product as a red solid (122 mg, 0.147 mmol, 86%). **^{1}H NMR** (400 MHz, $CDCl_3$): δ = 7.55 (d, J = 8.1 Hz, 2H), 7.46 (d, J = 8.7 Hz, 2H), 7.37 (d, J = 7.9 Hz, 2H), 6.95 – 6.82 (m, 6H), 6.48 (d, J = 3.6 Hz, 2H), 6.33 (d, J = 3.5 Hz, 2H), 3.84 (s, 6H), 2.67 (t, J = 7.6 Hz, 2H), 2.51 (s, 3H), 1.62 – 1.55 (m, 4H), 1.34 – 1.23 (m, 12H), 0.89 – 0.84 (m, 3H).**^{13}C NMR** (126 MHz, $CDCl_3$) δ = 160.51, 155.66, 145.42, 143.20, 140.75, 134.56, 133.68, 131.94, 131.68, 130.78, 129.31, 128.32, 126.24, 124.81, 124.37, 124.02, 113.60, 55.30, 31.68, 31.66, 30.15, 28.88, 22.69, 21.66, 14.21.**^{11}B NMR** (128 MHz, $CDCl_3$): δ = 0.81 (t, J_{B-F} = 30.7 Hz). **^{19}F NMR** (376 MHz, $CDCl_3$): δ = -134.3 (q, J_{B-F} = 30.5 Hz). **HRMS** (ESI-TOF): calcd for $C_{50}H_{53}BF_2N_2O_2S_2$ $[M]^+$, 826.3613; found 826.3565.

Synthesis of 7a

According to ***General Procedure 2*** with a slightly more excess of $FeCl_3$ (10 eq). Starting from **6a** (92 mg, 0.111 mmol). The reaction mixture was stirred 1 h at 0°C. Column chromatography (EP/DCM 1:1) followed by recrystallization by diffusion of EtOH in DCM afforded the pure **7a** (42.1mg, 0.0511 mmol, 46%) as a black solid. **^{1}H NMR** (400 MHz, $CDCl_3$): δ = 9.56 (d, J = 9.4Hz, 2H), 7.59 (d, J = 7.9 Hz, 2H), 7.52 (d, J = 2.8 Hz, 2H), 7.42 (d, J = 7.9 Hz, 2H), 7.39 (s, 2H), 7.31 (dd, J = 9.6, 2.8 Hz, 2H), 7.08 (s, 2H), 4.04 (s, 6H), 2.93 (t, J = 7.3Hz, 4H) , 2.56 (s, 3H), 1.76 (p, J = 7.5Hz, 4H), 1.38-1.46 (m, 4H), 1.31-1.36 (m, 8H), 0.88-0.92 (m, 6H). **^{13}C NMR** (100 MHz, $CDCl_3$): δ = 160.79, 150.17, 149.54, 145.36, 143.66, 140.61, 138.71, 134.74, 133.67, 132.40, 131.52, 130.35, 129.18, 126.85, 120.51, 120.02, 116.81, 114.65, 107.96, 55.67, 31.74, 31.62, 30.82, 28.92, 22.71, 21.68, 21.38, 14.23.**^{11}B NMR** (128 MHz, $CDCl_3$): δ = 2.82 (t, J_{B-F} = 34.8Hz). **19F NMR** (376 MHz, $CDCl_3$): δ = -140.03 (q, J_{B-F} = 35.1 Hz). **HRMS** (ESI-TOF): calcd for $C_{50}H_{49}BF_2N_2O_2S_2$ $[M]^+$, 822.3300; found 822.3361.

Aknowledgements:

FC thanks the University of Strasbourg and Ministry of Research for "contrat doctoral". GU and NL thanks the Centre National de la Recherche Scientifique and the University of Strasbourg in France for financial support. DJ is indebted to the CCIPL computational center for generous allocation of computational ressources.

Keywords: Dyes/Pigments ; BODIPY; Fluorescence; TD-DFT;

References

[1] G. Zhang, J. Zhao, P. C. Y. Chow, K. Jiang, J. Zhang, Z. Zhu, J. Zhang, F. Huang, H. Yan, *Chem. Rev.* **2018**, *118*, 3447–3507.
[2] A. D'Aléo, M. H. Sazzad, D. H. Kim, E. Y. Choi, J. W. Wu, G. Canard, F. Fages, J.-C. Ribierre, C. Adachi, *Chem. Commun.* **2017**, *53*, 7003–7006.
[3] K. Kolmakov, V. N. Belov, J. Bierwagen, C. Ringemann, V. Müller, C. Eggeling, S. W. Hell, *Chem. – Eur. J.* **2010**, *16*, 158–166.
[4] G. Ulrich, R. Ziessel, A. Harriman, *Angew. Chem. Int. Ed.* **2008**, *47*, 1184–1201.
[5] C. Jiao, K.-W. Huang, J. Wu, *Org. Lett.* **2011**, *13*, 632–635.
[6] L. Zeng, C. Jiao, X. Huang, K.-W. Huang, W.-S. Chin, J. Wu, *Org. Lett.* **2011**, *13*, 6026–6029.
[7] L. Jean-Gérard, W. Vasseur, F. Scherninski, B. Andrioletti, *Chem. Commun.* **2018**, *54*, 12914–12929.
[8] H. Lu, S. Shimizu, J. Mack, Z. Shen, N. Kobayashi, *Chem. – Asian J.* **2011**, *6*, 1026–1037.
[9] W. Sheng, Y.-Q. Zheng, Q. Wu, Y. Wu, C. Yu, L. Jiao, E. Hao, J.-Y. Wang, J. Pei, *Org. Lett.* **2017**, *19*, 2893–2896.
[10] A. Loudet, K. Burgess, *Chem. Rev.* **2007**, *107*, 4891–4932.
[11] N. Boens, B. Verbelen, M. J. Ortiz, L. Jiao, W. Dehaen, *Coord. Chem. Rev.* **2019**, *399*, 213024.
[12] K. Umezawa, A. Matsui, Y. Nakamura, D. Citterio, K. Suzuki, *Chem. - Eur. J.* **2009**, *15*, 1096–1106.
[13] S. G. Awuah, J. Polreis, V. Biradar, Y. You, *Org. Lett.* **2011**, *13*, 3884–3887.
[14] Y. Sun, Z. Qu, Z. Zhou, L. Gai, H. Lu, *Org. Biomol. Chem.* **2019**, *17*, 3617–3622.
[15] Z. Zhou, J. Zhou, L. Gai, A. Yuan, Z. Shen, *Chem. Commun.* **2017**, *53*, 6621–6624.
[16] L. Luo, D. Wu, W. Li, S. Zhang, Y. Ma, S. Yan, J. You, *Org. Lett.* **2014**, *16*, 6080–6083.
[17] X. Zhou, Q. Wu, Y. Feng, Y. Yu, C. Yu, E. Hao, Y. Wei, X. Mu, L. Jiao, *Chem. – Asian J.* **2015**, *10*, 1979–1986.
[18] D. Wang, C. Cheng, Q. Wu, J. Wang, Z. Kang, X. Guo, H. Wu, E. Hao, L. Jiao, *Org. Lett.* **2019**, *21*, 5121–5125.
[19] J. L. Belmonte-Vázquez, E. Avellanal-Zaballa, E. Enríquez-Palacios, L. Cerdán, I. Esnal, J. Bañuelos, C. Villegas-Gómez, I. López Arbeloa, E. Peña-Cabrera, *J. Org. Chem.* **2019**, *84*, 2523–2541.
[20] Y. Hayashi, N. Obata, M. Tamaru, S. Yamaguchi, Y. Matsuo, A. Saeki, S. Seki, Y. Kureishi, S. Saito, S. Yamaguchi, H. Shinokubo, *Org. Lett.* **2012**, *14*, 866–869.
[21] Q. Huaulmé, A. Sutter, S. Fall, D. Jacquemin, P. Lévêque, P. Retailleau, G. Ulrich, N. Leclerc, *J. Mater. Chem. C* **2018**, *6*, 9925–9931.
[22] Q. Huaulmé, S. Fall, P. Lévêque, G. Ulrich, N. Leclerc, *Chem. – Eur. J.* **2019**, *25*, 6613–6620.
[23] W. Miao, Y. Feng, Q. Wu, W. Sheng, M. Li, Q. Liu, E. Hao, L. Jiao, *J. Org. Chem.* **2019**, *84*, 9693–9704.
[24] M. J. Ortiz, A. R. Agarrabeitia, G. Duran-Sampedro, J. Bañuelos Prieto, T. A. Lopez, W. A. Massad, H. A. Montejano, N. A. García, I. Lopez Arbeloa, *Tetrahedron* **2012**, *68*, 1153–1162.

[25] Z. Feng, L. Jiao, Y. Feng, C. Yu, N. Chen, Y. Wei, X. Mu, E. Hao, *J. Org. Chem.* **2016**, *81*, 6281–6291.
[26] D. J. Jones, B. Purushothaman, S. Ji, A. B. Holmes, W. W. H. Wong, *Chem. Commun.* **2012**, *48*, 8066.
[27] Y.-C. Wei, S. F. Wang, Y. Hu, L.-S. Liao, D.-G. Chen, K.-H. Chang, C.-W. Wang, S.-H. Liu, W.-H. Chan, J.-L. Liao, W.-Y. Hung, T.-H. Wang, P.-T. Chen, H.-F. Hsu, Y. Chi, P.-T. Chou, *Nat. Photonics* **2020**, *14*, 570–577.
[28] B. Le Guennic, D. Jacquemin, *Acc. Chem. Res.* **2015**, *48*, 530–537.
[29] S. Chibani, B. Le Guennic, A. Charaf-Eddin, A. D. Laurent, D. Jacquemin, *Chem. Sci.* **2013**, *4*, 1950.